COMPARISON OF LOCAL SOLAR CELL EFFICIENCY ANALYSIS PERFORMED BY DLIT AND CELLO

O. Breitenstein[1], J. Carstensen[2], A. Schütt[2], J.-M. Wagner[2]
[1]Max Planck Institute of Microstructure Physics, Weinberg 2, D-06120 Halle, Germany
[2]Christian-Albrechts-University, Faculty of Engineering, Kaiserstraße 2, D-24143 Kiel, Germany

ABSTRACT: The local efficiency parameters of readily processed solar cells can be investigated both by applying dark lock-in thermography (DLIT) and Solar Cell Local characterization (CELLO), which is a special bias-dependent lock-in variant of light beam-induced current (LBIC) imaging. While the DLIT investigation directly leads to local two-diode data, until now results of CELLO investigations were displayed in a different way. The main purpose of this work is to develop a transformation of CELLO-based maps into local dark power and current density maps, which allow a direct comparison of the two approaches for local efficiency analysis. The comparison on one and the same cell shows a very good qualitative correspondence. Both DLIT and CELLO detect basically the same local inhomogeneities in J_{01} and J_{02}. However, there are still differences in the quantitative values. The origin of these differences is discussed.

Keywords: Multi-Crystalline Silicon Solar Cell, Characterization, CELLO, Lock-In Thermography, Local Efficiency Analysis

1 INTRODUCTION

Solar cells, even if made from monocrystalline silicon material, are typically spatially inhomogeneous devices. At least the effective series resistance R_s is position-dependent, but usually also the local lifetime and the diode properties are distributed inhomogeneously. This holds in particular for multicrystalline silicon cells, which, until now, always show defect regions of poor crystal quality and low lifetime, surrounded by regions of relatively good lifetime. In these defect regions not only the short-circuit current density J_{sc} is reduced, but also the first diode saturation current density J_{01}, describing recombination in the bulk and at the surfaces, is locally increased. These defect regions may seriously degrade the dark characteristic of the whole device and limit e.g. V_{oc}. Under illumination at V_{oc} condition, the 'good' crystal regions generate net photocurrent, which flows back as a net dark current into the 'bad' crystal regions, mediated by horizontal balancing currents in the bulk and in the metallization layers. Therefore the local characterization of solar cells by appropriate imaging methods is essential for characterizing these inhomogeneities and evaluating their influence on solar cell efficiency.

Methods for imaging efficiency-relevant solar cell properties are e.g. dark lock-in thermography (DLIT [1]), electroluminescence and photoluminescence imaging (EL [2], PL [3]) and light beam-induced current imaging (LBIC [4]). A special extended variant of LBIC, implying lock-in detection at various frequencies, pulsed laser illumination at various wavelengths, measurement at various biases, and additional homogeneous illumination, is Solar Cell Local Characterization (CELLO [5]). All these methods are based on different physical principles. In DLIT the local dark current density is measured by detecting the local heating. Hence, this method is only based on the energy conservation law: Wherever electric power is dissipated, heat is generated. Hence, the vertical dark current can easily be measured by DLIT and is only little influenced by R_s. EL and PL imaging basically rely on the measurement of the local diode voltage, since the luminescence signal is exponentially dependent on this voltage; additionally, it depends on the effective base lifetime. If there were no series resistance R_s between grid and local diode, PL and EL could not deliver any information on the local dark current, since then the local bias would be the same everywhere and equal to the applied bias. Only by the existence of R_s these luminescence methods may deliver information on the local dark characteristic. Qualitatively the same holds for CELLO. Also here, if there were no R_s, the local dark current information would average out across the whole area by the horizontal balancing currents. Only by the existence of R_s the CELLO investigation may also deliver information on the local diode properties. Therefore the local series resistance plays a crucial role for the evaluation both of EL/PL and CELLO measurements, but less for DLIT.

Due to their different natures, the results of the different methods are displayed differently and are hardly compatible to each other. While DLIT allows to image the local two-diode parameters J_{01}, J_{02}, n_2, and $G_p = 1/R_p$ quite straightforwardly [6], for EL and PL hitherto only R_s and J_{01} could be displayed [7]. For CELLO the results have been usually displayed as local current- or voltage-modulation images at different biases and ratios between these. Recently, techniques have been developed to display the results of DLIT and PL images also in form of local diode efficiency parameters like V_{oc}, FF, and η [8-10]. Comparisons between such DLIT- and PL-based results have been published in [10, 11]. The goal of this contribution is to display also CELLO results in terms of local dark current and dissipated power densities, which allows now for the first time a direct quantitative comparison between CELLO- and DLIT-based results on one and the same sample. In particular, this kind of representation allows to analyze also CELLO data by using the 'Local I-V 2' method [8], which enables a very detailed local efficiency analysis of solar cells.

One serious problem for such a comparison is that the local series resistance R_s is handled differently for DLIT/EL/PL and CELLO: The evaluation methods used for the former techniques are all based on the local one- or two-diode-model. Here the local R_s (in units of Ωcm^2) is defined as the local voltage drop between terminal and local diode, divided by the local current density. Hence, these techniques assume that each image pixel is connected with the terminal by its own and independent series resistance. This model actually may be wrong,

since the dominant part of the series resistance is a distributed resistance, see [12]. However, it regards the horizontal balancing currents mentioned above. It only assumes that these currents all go from a net current source across the busbars to a net current sink. Thereby, the series resistance for these currents is certainly overestimated, since in reality these currents take the shortest route. In CELLO, on the other hand, the local R_s (in units of Ω) is defined as the difference between the local voltage and the terminal voltage, divided by the total cell current. If the diode properties are homogeneous, R_s^{CELLO} is correctly converted into the conventional R_s by multiplying it with the cell area, since in a homogeneous cell the local dark current density basically equals the global one. Here we have used this rule, knowing that it is only an approximation, since our cell is inhomogeneous.

2 METHODS AND EXPERIMENTS

2.1 DLIT-based analysis

The DLIT-based local efficiency analysis is based on the procedure for local analysis of current-voltage characteristics proposed in [6]. Like any other quantitative evaluation of DLIT data, it relies on the proportionality of the *T*-modulation signal component being –90° phase shifted to the applied bias pulses to the locally dissipated power density p. In the procedure proposed in [6] three DLIT images taken at three different forward biases (e.g. 0.5, 0.55, and 0.6 V) plus one image taken at a low reverse bias (e.g. –1 V) are evaluated. Here an image of the local R_s must be entered into the procedure, which may be assumed to be constant or may come e.g. from an EL or PL evaluation of the investigated cell. Alternatively, R_s may also be obtained by applying the so-called RESI method, which was proposed by Ramspeck et al. [13]. Here, for the highest forward bias, where R_s is most disturbing, the local p-n junction voltage is obtained by evaluating two EL images of different biases, e.g. according to [14], and the locally dissipated power density is measured by DLIT. The combination of these data leads to values of the local current density J and of R_s, which allow to calculate the local p-n junction voltage V_{loc}. It turns out that the DLIT-based analysis is only little disturbed by the distributed character of R_s, since here the current is measured more directly. This measurement even works best for $R_s = 0$, only for very large values of R_s (above 3 ... 10 Ωcm^2) it may become inaccurate. Then the $J(V_{loc})$ data are fitted for each pixel to the two-diode model, leading to local values of J_{01}, J_{02}, n_2, and R_p resp. $G_p = 1/R_p$. In this procedure the ideality factor of the first diode n_1 may be chosen larger than unity for the whole cell, which may account for an injection-intensity dependent lifetime [15, 16].

Based on the basic version of this procedure [6], an extended version has been developed, which allows one to load a J_{sc} image and enables the simulation of local dark and illuminated characteristics including the influence of R_s [8]. This new procedure calculates e.g. local p-n junction voltage and current density images at any applied voltage including V_{mpp}. Thereby it also calculates the locally contributing efficiency, which is the product of V_{mpp} and the local current density at mpp(cell). In addition, the procedure simulates the properties of selected pixels or extended regions under the assumption that they are electrically isolated. Thus, it also generates images of the efficiency parameters V_{oc}, FF, and the efficiency η, which correspond to the efficiency 'potential' of the selected region. Moreover, it generates images of the 'pseudo fill factor' and 'suns efficiency', which hold for the local diodes or regions without any R_s. From any region, including the whole cell, dark and illuminated *J–V* characteristics and also suns-V_{oc} characteristics (without the influence of R_s) can be obtained, and the corresponding efficiency parameters V_{oc}, FF, V_{mpp}, J_{mpp}, and η are calculated. A software package called 'Local I-V 2' containing this DLIT data evaluation procedure is available [17]. The experimental DLIT results shown here have been obtained on a typical industrial multicrystalline silicon solar cell by using a Thermosensorik TDL 640 S/M system. The total acquisition time for all four images used was about 2 hours.

2.2 CELLO-based analysis

The CELLO system measures the linear photo-current and/or photo-voltage response to local laser illumination for laser wavelengths of 650 nm, 830 nm, and 934 nm (and, therefore, different penetration depths of light into Si), various intensity modulation frequencies between 6 kHz and 22 kHz, and at different points along the *I–V* curve. In this study 24 maps of short-circuit current maps (amplitude and phase shift) have been used for a fit to the diffusion equation to calculate local maps of the bulk lifetime τ and the surface recombination at the back side S_B [5].

To calculate the $J_{01}(x,y)$ map, these local data have been used as input for solving the stationary diffusion equation for $\Delta n = n - n_0$ with the boundary condition $n(z = 0) = 0$, i.e. $\Delta n(z = 0) = -n_0$, corresponding to the condition of extracting all free minority carriers (generated in the dark) at the front side by applying reverse bias in saturation. The current extracted from the front side for this boundary condition is just $J_{01}(x,y)$. Assuming a constant doping of the Si wafer, i.e. a constant n_0, the value of n_0 has been calculated by fixing the average of the $J_{01}(x,y)$ map to the J_{01} value extracted from the fit to the global *I–V* curve of the solar cell. From the so-determined value of n_0 and temperature-dependent value of n_i, a value of $N_A = n_i^2/n_0 = 3.6 \times 10^{16}$ / cm^3 has been found, which is in very good agreement to $N_A = 4 \times 10^{16}$ / cm^3 calculated from the specific resistivity of the Si wafer.

The CELLO series resistance map $R_{s,\infty}(x,y)$ used in this paper has been obtained from the impedance fit to short-circuit current maps as well. In order to get consistent results to the CELLO data under forward bias the resistance maps have to be modified according to

$$\frac{1}{R_s^{CELLO}(x,y,V)} = \frac{1}{R_{s,\infty}^{CELLO}(x,y)} + \left\langle \frac{1}{R_D(V)} \right\rangle . \quad (1)$$

Here $< 1 / R_D(V) >$ is the slope of the first diode which can directly be calculated from the fit of the global *I–V* curve. In contrast to the local two-diode model (i.e. completely independent neighboring points) used for the DLIT analysis, the CELLO series resistance model uses an approximation starting from the perfect grid (i.e. a perfect equipotential layer) and thus completely dependent neighboring points. For this approximation Eq. (1) is a must, taking into account that in forward direction an increasing fraction of the (photo-)current is short-

circuited by the local diodes, thus reducing the fraction of current which has to pass through the grid network and consequently also reducing the ohmic losses related to this network. Equation (1) has been found to hold (in a somewhat averaged version) for nearly all solar cells analyzed using the CELLO technique and luminescence data [18, 19]. Like the model of independent diodes this approach does not take fully into account horizontal balancing currents (e.g. induced by an inhomogeneous lifetime distribution), which can vary strongly along the *I–V* curve. The decisive difference between both models shows up for the calculation of local voltage maps which for the CELLO model is calculated by

$$V(x,y) = V_{\mathrm{ext}} - R_{\mathrm{s}}^{\mathrm{CELLO}}(x,y,V)\, I_{\mathrm{ext}} \,. \qquad (2)$$

Here V_{ext} is the externally applied (terminal) voltage and I_{ext} the externally induced/extracted global current. This equation emphasizes the non-local origin of the current flow, leading to local ohmic losses, while for the model of independent diodes a purely local current density $J(x,y)$ is assumed as the (only) reason for ohmic losses.

Combining a photo-current map at the maximum power point of the solar cell, $dI_{\mathrm{mpp}}(x,y)$, a short-circuit current map, $dI_{\mathrm{sc}}(x,y)$, the $J_{01}(x,y)$ map, and the $R_{\mathrm{s}}(x,y,V_{\mathrm{mpp}})$ map, the $J_{02}(x,y)$ map is calculated in a straightforward manner (details will be discussed elsewhere). All measurement artifacts or imperfections in modeling the data thus will show up in the J_{02} map. With all these maps at hand, it is straightforward to also calculate local dark power density maps. Measuring the 25 maps which contain much more information necessary for the discussion presented in this paper takes roughly one hour.

3 RESULTS

3.1 Input data

In Fig. 1 original CELLO maps used to calculate the CELLO dark power maps in Fig. 2 are shown. A set of 24 photo-current maps (amplitude and phase; an example is shown in Fig. 1 (a, b)), measured with three different laser wavelengths and for four different modulation frequencies, is used as input for an impedance analysis [5], resulting, among others, in maps of diffusion length and back surface recombination velocity, shown in Fig. 1 (c, d). The measured phase shift is determined by time constants related the extraction of the photocurrent: low bulk lifetime leads to small absolute phase shifts (appearing bright in Fig. 1 (b); note that phase values are negative), while a low mobility leads to increased phase values (not found in Fig. 1 (b)), and a high series resistance leads to large phase shifts (present at some of the darkest parts in Fig 1(b); cf. Fig. 2 (f)).

CELLO is essentially a tool for locally analyzing solar cell losses under illumination. Thus it is easy to separate bulk lifetime loss contributions to J_{01} from losses at the back side of the solar cell. This has been summarized in Fig. 1 (e) showing the fraction of bulk losses relative to the sum of bulk and S_{B} losses. Clearly the right and upper part of the solar cell show smaller diffusion lengths and thus a larger fraction of bulk losses.

In addition Fig. 1 (f) shows the global illuminated and dark *I–V* curve as measured in the CELLO setup and the reconstructed *I–V* curves using the J_{01}-, J_{02}-, and R_{s}-maps (in combination with Eq. (1)), and n_2 = 2.48 as extracted from the fit to the global *I–V* curve.

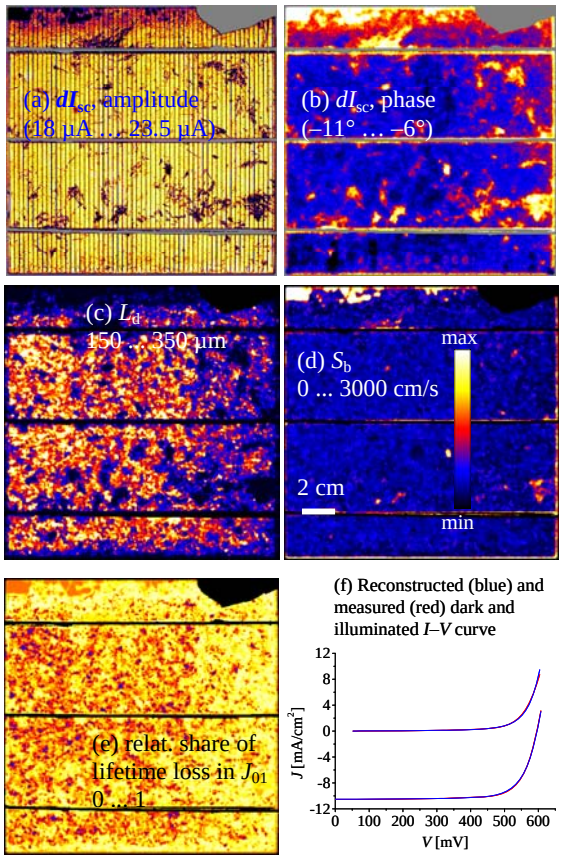

Fig. 1: CELLO data for dark current analysis. (a, b): photocurrent maps (a: amplitude, b: phase) measured by an IR laser; (c, d): impedance fit results as input for J_{01} calculation (c: diffusion length, d: back surface recombination velocity); (e) resulting relative share of lifetime loss in J_{01}; (f) reconstruction (blue) of measured (red) dark and illuminated *I–V* curve.

This nearly perfect agreement between the local and global CELLO results is only possible using the distributed R_{s} model, i.e. incorporating the voltage dependence of the series resistance using Eq. (1). The reason for this quite obviously lies in the exponential terms $\exp(qV(x,y)/kT)$ in the diode equation. While J_{01} and J_{02} are linear factors in the diode equation, the series resistance leads to strongly non-linear contributions. Averaging local *I–V* curves incorporating the local voltage distribution $V(x,y)$ can only lead to a consistent global *I–V* curve if $V(x,y)$ is constant, i.e. $R_{\mathrm{s}}(x,y) = 0$, or taking into account Eq. (1), at least when calculating the local voltage distribution according to Eq. (2).

In Fig. 2 the typical dark *I–V* input data of the DLIT and of the CELLO measurements are shown, which are images of the local power density p at about 0.5 and 0.6 V and of the contributing series resistance R_{s}. Note that this analysis is based on the local two-diode model, hence it is assumed that each pixel is connected with the terminals by an independent and constant series resistance. Note also that in the CELLO-based images the data of the upper right corner region are replaced by data from its surrounding, since this corner was broken out between the DLIT and the CELLO investigation.

The DLIT-based power density images taken at 0.55 and –1 V, which were also used for the evaluation, are not shown here. For DLIT, the power density images come directly out of the measurement, and for CELLO

they have been obtained by the procedure described in Sect. 2.2. For CELLO, the R_s image also results from this analysis, whereas for DLIT the R_s image results from the evaluation of two additional EL images according to the RESI methods of Ramspeck [13] or the EL evaluation method of Breitenstein [14].

At 0.5 V bias the depletion region recombination current is expected to dominate in the local power density images, but at 0.6 V the so-called diffusion current, which is due to recombination in the bulk and at the surfaces, is expected to dominate. Indeed, the bright local shunts visible in Fig. 2 (a) and (b) are so-called 'J_{02}-type shunts', which are due to extended defects crossing the p-n junction, see Sect. 3.3. The larger size of these shunts in (a) is due to thermal blurring. The 0.6 V images (c) and (d) are more dominated by the local lifetime in the bulk, though they still contain the J_{02} shunts. The DLIT- and CELLO-based p images are similar but not identical. This holds also for the two R_s images (e) and (f). Due to the special R_s concept of the CELLO procedure, the CELLO-R_s image (f) does not show any inhomogeneity due to the inhomogeneous bulk lifetime, whereas the RESI-R_s image (e) does. These differences will be discussed in Sect. 4.

3.2. Global results

All results shown below are outputs of the 'Local I-V 2' procedure [8], which allows to simulate also the global characteristic of a whole spatially inhomogeneous solar cell, based on the CELLO- and DLIT-based primary dark I–V results as shown in Sect. 3.1. One of the options is to display simulated 'suns-V_{oc}' characteristics. This is the dark characteristic of all cell pixels switched in parallel without any series resistance. In this representation the characteristics may be split into a diffusion current (first diode) and a recombination current (second diode) component. Fig. 3 shows the comparison of the DLIT- and CELLO-based suns-V_{oc} characteristics, where the recombination current is shown in green and the diffusion current dashed. The data points are the measurement points. The comparison shows that the DLIT analysis leads to a somewhat higher diffusion current, with the recombination current being about the same for both, just having a higher ideality factor for the DLIT analysis (for CELLO, n_2 = 2 had to be assumed in the 'Local I-V 2' procedure, since only two input maps were used). In this cell the ohmic shunt current is negligible

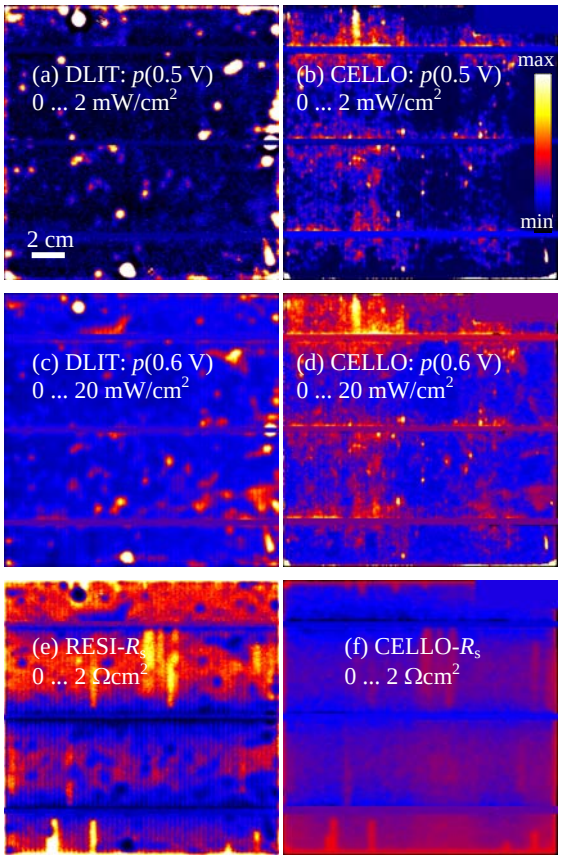

Fig. 2: DLIT- and CELLO-based local power density and series resistance images.

Figure 4 shows part of the illuminated characteristics close to mpp according to the flasher data and the 'Local I-V 2' simulations resulting from the DLIT- and CELLO-based local dark I–V data, all assuming the same (measured) homogeneous J_{sc} = 31.8 mA/cm^2. Near the respective mpp-points, which are lying between 0.51 and 0.53 V, the curves are lying close together. The CELLO-based 'Local I-V 2' analysis predicts a slightly too high V_{oc}. The global solar cell data are summarized for both simulations in Tab. 1. These data confirm the qualitative differences shown in Fig. 4.

3.3. Local dark I–V results

The power density images at about 0.5 and 0.6 V shown in Fig. 2 still contain both J_{01}- and J_{02}-contributions, even though in different degrees. The 'Local I-V 2' procedure allows a separation of these two components based on the two-diode model. Thereby the DLIT-based analysis assumes a variable ideality factor of the recombination current n_2, whereas here for the CELLO-based analysis n_2 = 2 was used. Then it is not useful to image J_{02} as a local measure of the recombination current. Therefore in Fig. 5 the simulated dark current densities for the diffusion and for the recombination current are shown for the highest measured bias, which was in both cases close to 0.6 V. Figure 5 shows that both for the DLIT- and for the CELLO-based analysis the distinct bright spots (shunts) are indeed all J_{02}-type (recombination current) shunts, hence these are extended defects crossing the p-n junction. Also the depletion region recombination in the edge region, particularly at the lower right edge, is visible in both techniques, see also Fig. 2 (a) and (b).

As already mentioned, the generally larger size of the shunts in the DLIT analysis is due to the inevitable thermal blurring. However, the intensity (brightness) of these shunts is different for both types of analysis. In particular, the two strong shunts at the top and at the bottom, which are dominating in the DLIT-based J_{rec} image Fig. 5 (a), appear in the CELLO-based image (b) not stronger than the other shunts. Moreover, only in the CELLO-based J_{rec} image (b), extended regions of J_{02} current exist in the left part of the cell, which appear to be stronger close to the busbars.

Tab. 1: Summary of the global cell data

	flasher data	DLIT-based	CELLO-based
J_{01} [A/cm^2]		8.29×10^{-13}	5.55×10^{-13}
V_{oc} [mV]	625	624	631
FF [%]	76.5	77.6	77.4
efficiency [%]	15.2	15.4	15.5

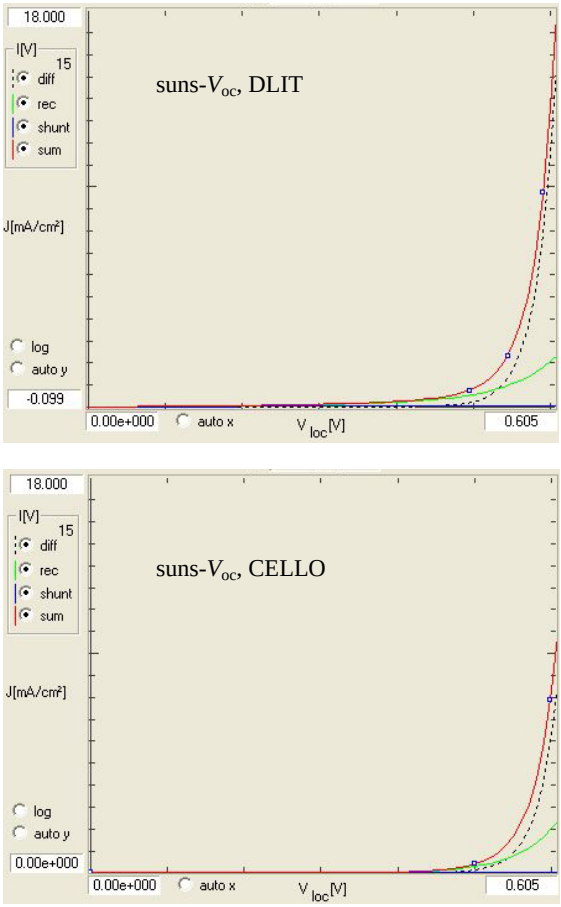

Fig. 3: DLIT-based (top) and CELLO-based simulated global suns-V_{oc} characteristic (bottom).

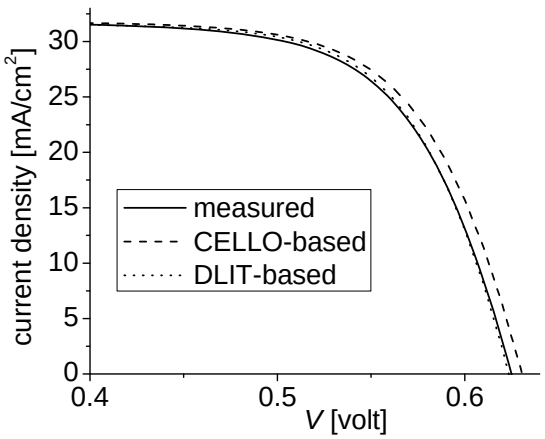

Fig. 4: Measured versus simulated (by 'Local I-V 2') illuminated *I–V* data close to mpp.

These can be consequences of the CELLO data evaluation as mentioned above: In CELLO the starting point for obtaining the J_{02} image is the dI_{mpp} map, taken under conditions where horizontal balancing currents flow into the regions of lower quality at the upper edge and the right part of the solar cell, cf. Fig. 1 (c, e). These currents act as losses for the good regions of the solar cell. Therefore, the extended J_{02} features in Fig. 5 (b) can be consequences of an injection-level dependence of the volume lifetime or horizontal balancing currents.

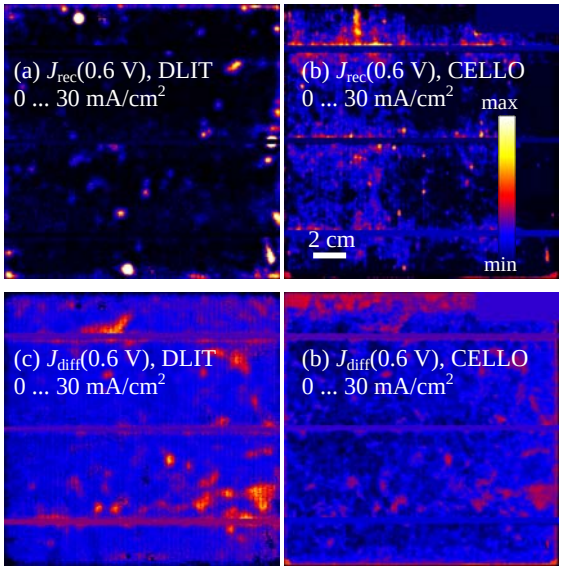

Fig. 5: DLIT- and CELLO-based dark current images.

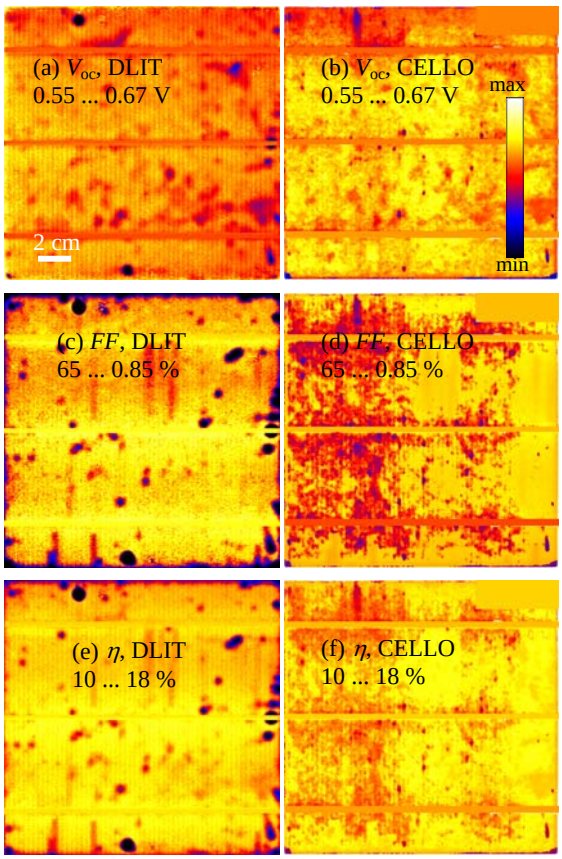

Fig. 6: DLIT- and CELLO-based local solar cell parameter images.

The inhomogeneities in the diffusion current images are inhomogeneities of J_{01}, which correlate to recombination-active lattice defects. Since the CELLO-based analysis predicts a generally lower value of J_{01} (see Fig. 4 and Tab. 1), the maxima of J_{diff} are weaker in Fig. 5 (d) than in (c). In a horizontal region below the upper cell edge, CELLO predicts an extended region of increased J_{01}, which is only weakly visible in the DLIT

analysis. This region was visible on this cell already earlier in luminescence images [20]. The nature of these defects, which obviously appear in luminescence and LBIC resp. CELLO images, but not in DLIT images, is not clear yet.

3.4. Images of solar cell parameters

As mentioned in Sect. 2.1. there are two possibilities to image local solar cell parameters. The first one is to consider the solar cell as it is. Hence, it is assumed that all regions are electrically coupled to each other by the lateral series resistances. If the whole cell is under illumination, e.g. at V_{mpp} or at V_{oc}, in an inhomogeneous cell there are horizontal balancing currents, which lead excess photocurrent from good cell regions to some shunt regions, where it flows back as dark current. Then only some regions of the cell are under their individual mpp- or open circuit voltage, in good regions being higher and in poor regions lower than V_{mpp} or V_{oc} of the whole cell, respectively. The second possibility is to consider each pixel as an electrically isolated region. Then, by knowing the dark current parameters and the individual R_s and J_{sc} values, the 'Local I-V 2' procedure calculates the individual illuminated *I-V* characteristic of each pixel and thus obtains their local 'expectation' or 'potential' values of V_{oc}, fill factor FF, and the efficiency η. Only by this kind of representation the question can be answered how good a solar cell could be if it were everywhere as good as in its best region. Therefore in this work this latter kind of display of the results was chosen, though the 'Local I-V 2' procedure also may apply the first possibility.

In Fig. 6 the images of V_{oc}, FF, and η are compared between the DLIT- and the CELLO-based analysis. In all cases a homogeneous distribution of J_{sc} equal to its measured mean value of 31.8 mA/cm^2 was assumed. As it was indicated in Tab. 1, CELLO predicts a slightly too high V_{oc} when evaluating the CELLO data with constant local series resistances along the *I-V* characteristic. Using the model of a voltage-dependent distributed series resistance, however, the illuminated *I–V* characteristic is reproduced very well by the CELLO analysis, see Fig. 1 (f).

Whereas for DLIT the fill factor is dominated by R_s and the local J_{02} shunts, for CELLO it is also dominated by the homogeneous J_{02} regions discussed above. These differences are also reflected in the resulting efficiency image, which is basically the product of the V_{oc} and the FF image. It turns out that the DLIT analysis leads to the prediction of fewer defects occupying a smaller area fraction, but there they have locally a stronger influence on the efficiency than that predicted by the CELLO analysis.

4 DISCUSSION

It should be pointed out that this whole analysis is generally not exact but is based on some approximations. The most serious one is probably the application of the local two-diode model, which assumes an independent and constant series resistance from the terminal to each pixel. As mentioned above, in reality the grid and emitter resistances yield a 2-dimensional network and the series resistance is mainly a distributed resistance, see [12]. This leads to the fact that the current through one region also influences the local voltage in the surrounding regions. The local two-diode model, on the other hand, is based on the area-related definition of a series resistance, which neglects any direct interaction between the pixels and is therefore a very coarse approximation. Nevertheless, also this approximation may describe the local voltage drops correctly, at least for a certain biasing and illumination condition of the cell. Therefore the results of this analysis, though not being exact, are certainly very useful.

It was already mentioned that CELLO and DLIT are relying on different R_s concepts. The RESI-R_s image used for DLIT measures the local voltage drop at the highest voltage (here 0.6 V) by EL and the locally dissipated power density by LIT imaging and calculates from this the local resistance [13]. If there is a local shunt, it pulls down the local voltage there and in its surrounding. However, since the current flows into this shunt region from all four sides, the amount of this voltage drop is lower than for a spatially extended shunting region, where the current comes only from one direction (from the busbars). Therefore the RESI-R_s value is generally lower at local defect (shunt) positions, as can be seen in Fig. 2 (e). In contrast the CELLO-R_s model uses Eq. (2) for calculating ohmic losses, no pure local current contribution to the ohmic losses are assumed. Therefore Fig. 2 (f) does not reflect the current density features but reflects more the pure ohmic features of the grid network.

Generally, the DLIT- and CELLO-based analysis both come to the same conclusions: In the best regions, this cell has the potential to deliver an efficiency of about 16.2 %, compared to the real cell efficiency of 15.2 %. This difference is caused, besides the influence of R_s, by extended defect regions of low bulk lifetime, with increased J_{01}, and by local J_{02}-type shunts, which are located at the cell edge and in some spots in the cell area, where most probably extended defects are crossing the p-n junction.

The reasons for the remaining quantitative differences between the DLIT- and CELLO-based local efficiency analysis are still under investigation. It must be considered that these are completely different imaging techniques. Insofar the strong correlations between the results of both techniques are already remarkable. A similar comparison has recently been made between DLIT- and photoluminescence (PL)-based local efficiency analysis [11]. Here it was found that the J_{02} inhomogeneities predicted by PL did not correlate at all to that found by DLIT. Most probably the reason for this discrepancy, as well as for the remaining discrepancies between the DLIT- and CELLO-based analysis reported here, is the used R_s model and the influence of the horizontal balancing currents. Only DLIT images the local currents directly, whereas for PL resp. CELLO the local dark characteristic just influences the luminescence resp. generated current signal, mediated and strongly influenced by the complex series resistance. It is hoped that these processes will become better understood in future, leading to an even better correspondence between local efficiency analysis performed by various methods.

Acknowledgements

This work was partially supported by the German Federal Ministry for the environment (BMU) through the 'SolarWinS' project, contract 0325270C, and the Deutsche Forschungsgemeinschaft, project FO 258/11-2.

References

[1] O. Breitenstein, W. Warta, M. Langenkamp, Lock-in Thermography - Basics and Use for Evaluating Electronic Devices and Materials (second edition), Springer (Heidelberg / New York) 2010.
[2] T. Fuyuki, H. Kondo, T. Yamazaki, Y. Uraoka, Appl. Phys. Lett. 86 (2005) 262108.
[3] T. Trupke, R.A. Bardos, M.C. Schubert, W. Warta, Appl. Phys. Lett. 89 (2006) 044107.
[4] J. Marek, J. Appl. Phys. 55 (1984) 318.
[5] J. Carstensen, A. Schütt, G. Popkirov, H. Föll, Phys. Status Solidi C 8(4) (2011) 1342.
[6] O. Breitenstein, Sol. Energy Mater. & Sol. Cells 95 (2011) 2933.
[7] M. Glatthaar, J. Haunschild, R. Zeidler, M. Demant, J. Greulich, B. Michl, W. Warta, S. Rein, R. Preu, J. Appl. Phys. 108 (2010) 014501.
[8] O. Breitenstein, Sol. Energy Mater. & Sol. Cells 107 (2012) 381.
[9] C. Shen, H. Kampwerth, M. Green, T. Trupke, J. Carstensen, Sol. Energy Mater. & Sol. Cells 109 (2013) 77.
[10] C. Shen, H. Kampwerth, M.A. Green, T. Trupke, O. Breitenstein, M. Zhang, Sol. Energy Mater. & Sol. Cells, submitted.
[11] O. Breitenstein, C. Shen, H. Kampwerth, M.A. Green, Energy Procedia 38 (1013) 2.
[12] G. Araujo, A. Cuevas, J.M. Ruiz, IEEE Transact. Electron Dev. 33 (2007) 093506.
[13] K. Ramspeck, K. Bothe, D. Hinken, B. Fischer, J. Schmidt, R. Brendel, Appl. Phys. Lett. 90 (2007) 153502.
[14] O. Breitenstein, A. Khanna, Y. Augarten, J. Bauer, J.-M. Wagner, K. Iwig, Phys. Status Solidi RRL 4 (2010) 7.
[15] D. Macdonald, A. Cuevas, Prog. Photovolt: Res. Appl. 8 (2000) 363.
[16] S. Rißland, O. Breitenstein, Sol. Energy Mater. & Sol. Cells 111 (2013) 112.
[17] <http://max-planck-innovation.de/en/>
[18] J.-M. Wagner, J. Carstensen, A. Berhane, A. Schütt, H. Föll, in Proc. 26th European Photovoltaic Solar Energy Conference, Hamburg (2011) 2BV.2.51.
[19] J.-M. Wagner, M. Hoppe, A. Schütt, J. Carstensen, H. Föll, Energy Procedia 38 (2013) 199.
[20] O. Breitenstein, J. Bauer, K. Bothe, D. Hinken, J. Müller, W. Kwapil, M.C. Schubert, W. Warta, IEEE J. Photovolt. 1 (2011) 159.